

# Pros and cons of structural chirality measurements and computation of handedness in periodic solids

Fernando Gómez-Ortiz,<sup>1,\*</sup> Mauro Fava,<sup>1</sup> Emma E. McCabe,<sup>2</sup> Aldo H. Romero,<sup>3</sup> and Eric Bousquet<sup>1</sup>

<sup>1</sup>*Physique Théorique des Matériaux, QMAT, CESAM, Université de Liège, B-4000 Sart-Tilman, Belgium*

<sup>2</sup>*Department of Physics, Durham University, South Road, Durham, DH1 3LE, U. K.*

<sup>3</sup>*Department of Physics and Astronomy, West Virginia University, Morgantown, WV 26505-6315, USA*

(Dated: May 29, 2024)

We compare the various chirality measures most widely used in the literature to quantify chiral symmetry in extended solids, i.e., the continuous chirality measure, the Hausdorff distance, and the angular momentum. By studying these functions in an algebraically tractable case, we can evaluate their strengths and weaknesses when applied to more complex crystals. Going beyond those classical calculations, we propose a new method to quantify the handedness of a crystal based on a pseudoscalar function, i.e., the helicity. This quantity, borrowed from hydrodynamics, can be computed from the eigenvector carrying the system from the high-symmetry non-chiral phase to the low-symmetry chiral phase. Different model systems like  $K_3NiO_2$ ,  $CsCuCl_3$  and  $MgTi_2O_4$  are used as test cases where we show the superior interest of using helicity to quantify chirality together with the handedness distinction.

## I. INTRODUCTION

A recent revival of chirality studies in materials has occurred due to its applicability in high-impact fields like topological insulators or chiral phonons in 2D materials [1]. Despite this revival, relatively little attention has been paid to the structural chirality in crystalline phases. From a symmetry standpoint, the criteria for a crystal to exhibit chirality are straightforward: it must lack improper rotation symmetry elements within its symmetry group (i.e. no "operations of the second kind" which can convert right-handed coordinate systems into left-handed ones) [2]. This condition leads to a comprehensive classification of the 230 crystallographic space groups [1, 3]. The first category encompasses 165 space groups which include improper symmetry operations, rendering them achiral. The second category comprises the remaining 65 groups, called Sohncke space groups, which are exclusively characterized by containing orientation-preserving operations (i.e. only "operations of the first kind") [2]. Among the Sohncke groups, we can further distinguish two different subcategories: 11 enantiomorphic pairs (22 chiral groups) characterized by containing screw axis of opposite handedness and 43 non-enantiomorphic space groups that will only preserve the chirality of the motif. The former subset of space groups will be the focus of this work.

However, this binary (chiral vs. achiral) classification sometimes proves insufficient, particularly when we aim to identify materials with optimal chiral responses for specific functionalities such as optoelectronics [4]. A more nuanced approach involves categorizing crystals based on their varying degrees of chirality, offering a richer classification of materials [5, 6]. To address this

challenge, significant efforts have been dedicated in the literature to continuously quantify chirality over the past few years despite its inherent difficulty [7–9]. Evidence of such attempts can be found in various measures, including the continuous chirality measure [5, 6], the Hausdorff distance [1, 10], or the phonon pseudo-angular momentum of the eigendisplacements [11]. Chirality measures are commonly divided into two primary categories based on their mathematical behavior under symmetry transformations: scalar and pseudoscalar functions. Scalar functions retain their value when subjected to mirror symmetry, making them invariant under such transformations. In contrast, pseudoscalar functions are sensitive to these symmetries and undergo a sign change when reflected. Intriguingly, in structural chirality determination, scalar functions are predominantly utilized in most established measures. This prevalence overshadows pseudoscalar functions, which remain relatively unexplored and elusive to the best of our knowledge.

In this study, we delve into the strengths and weaknesses of the previously announced chirality measures, e.g., the continuous chirality measure, the Hausdorff distance, and the pseudo-angular momentum. Going further, we propose a fresh methodology to determine the handedness of crystalline solids by utilizing a pseudoscalar function inspired by the concept of helicity in hydrodynamics [12, 13]. This innovative approach quantifies the degree of chirality in a crystal and distinguishes between right- and left-handed configurations. However, it is worth noting that while all handed objects are inherently chiral, not all chiral objects exhibit handedness [1]. Consequently, our proposed method effectively assesses the chiral response of any crystal within the 11 pairs of enantiomorphic space groups [14], albeit it poses problems to those within chiral non-enantiomorphic space groups, limiting its applicability.

The article is organized as follows. In the following section, we will inquire into the highly tractable scenario

---

\* fgomez@uliege.be

of a unit perovskite  $ABO_3$  cell, where all the various chiral measurements can be computed algebraically, providing a clear understanding of their limitations. Moreover, we shall introduce the concept of helicity as a new chiral measure to quantify the handedness of a crystalline structure. After identifying the strengths and weaknesses of the aforementioned quantities, we shall apply them to different cases of interest. Subsequent sections will therefore be dedicated to the particular study of  $K_3NiO_2$ ,  $Na_3AuO_2$ ,  $CsCuCl_3$ , and  $MgTi_2O_4$  that have been selected as paradigmatic examples.

## II. THE CASE OF A UNIT PEROVSKITE CELL

In this section, we present the continuous chirality measure, the Hausdorff distance, and the pseudo-angular momentum techniques through a simple toy model formed by an isolated  $ABO_3$  perovskite unit cell. This examination aims to delineate the applicability range of these approaches. Additionally, we shall introduce a new pseudoscalar measure to quantify the handedness of a given structure precisely.

### A. Problems with continuous chirality measurements

We begin by examining a simplified model system: a prototypical  $ABO_3$  perovskite unit cell, without considering its periodic replicas. In its centrosymmetric cubic phase, corresponding to the  $Pm\bar{3}m$  space group under hypothetical periodic boundary conditions, the crystal is inherently non-chiral, as illustrated in Fig. 1(a). Next, we introduce structural distortions to this system and analyze their impact on different chirality measurements. According to Hlinka, chirality can arise from the interaction of a vector  $V$  with a rotational mode  $R$ , forming an axial vector. Although these distortions, when considered separately, might be achiral, their coupling can lead to the emergence of chiral distortions [15].

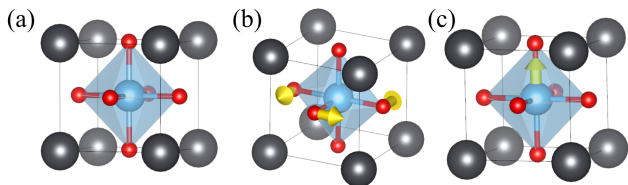


FIG. 1. Schematic view of the unit cell in the prototypical cubic  $ABO_3$  perovskite structure together with their dominant instabilities without periodic boundary conditions. (a) Non-polar cubic centrosymmetric phase. (b) Non-polar rotation of the oxygen octahedra. (c) The off-centering motion of the B atom. Grey, blue, and red balls represent A, B, and O atoms, respectively. Yellow arrows indicate the direction for the non-zero displacements.

These vector and rotation modes can be achieved in our model by the distortions schematized in Fig. 1. In particular, a local rotation in a perovskite can be obtained by a rotation of the oxygen octahedra [Fig. 1(b)], and a polar vector can be simplified by an off-centering of the B cation [Fig. 1(c)]. Such transformations are easy to characterize algebraically, and the values of the new positions of the distorted atoms can be found in the following Eq. (1):

$$\begin{aligned} O_{x1} &= \left(\frac{1}{2} - \frac{1}{2} \cos \theta, \frac{1}{2} - \frac{1}{2} \sin \theta, \frac{1}{2}\right), \\ O_{x2} &= \left(\frac{1}{2} + \frac{1}{2} \cos \theta, \frac{1}{2} + \frac{1}{2} \sin \theta, \frac{1}{2}\right), \\ O_{y1} &= \left(\frac{1}{2} + \frac{1}{2} \sin \theta, \frac{1}{2} - \frac{1}{2} \cos \theta, \frac{1}{2}\right), \\ O_{y2} &= \left(\frac{1}{2} - \frac{1}{2} \sin \theta, \frac{1}{2} + \frac{1}{2} \cos \theta, \frac{1}{2}\right), \\ B &= \left(\frac{1}{2}, \frac{1}{2}, \frac{1}{2} + \xi\right), \end{aligned} \quad (1)$$

where  $\theta$  is the rotation angle of the oxygen octahedra with respect to the  $z$ -axis and  $\xi$  is the off-centering of the B atom. We have, therefore, three different structures: i) the high-symmetry cubic phase (that would correspond to a  $Pm\bar{3}m$  space group with periodic boundary conditions), ii) the lower symmetry phase corresponding to the rotation of the oxygen octahedra (represented by a  $I4/mcm$  space group with periodic boundary conditions), and iii) the phase corresponding to the off-centering of the B cation (ascribed to a  $I4/mcm$  space group with periodic boundary conditions). Clearly, the two distortions are nonchiral individually, as they present mirror symmetry planes along  $z$  and  $x$ , respectively. However, when the octahedral rotation is combined with the off-centering motion of the B cation, a chiral structure emerges at the unit cell level as it combines a vector (polar distortion) and an axial vector (octahedra rotation). It is important to highlight that, in the periodic crystal, the antiferrodistortive coupling of the oxygen octahedra causes octahedra to rotate cooperatively in opposite directions from unit cell to unit cell. In contrast, the off-centering direction is preserved, leading to opposite chirality and an overall achiral system. The system would be antichiral unit-cell wise as the chirality from one unit cell will reverse sign but keep the same absolute value concerning its neighboring cells. Nevertheless, for the sake of simplicity in our analysis, we will restrict our examination to the chiral nature observed at the unit cell level in this straightforward scenario.

#### 1. Continuous Chirality Measure

The continuous chirality measure (CCM) is a scalar measure introduced by Avnir that quantifies the struc-

ture's distance to its closest achiral reference [6]. Mathematically, it can be expressed as:

$$\text{CCM} = \frac{1}{N} \sum_1^N \|\vec{x}_i - \vec{x}'_i\|^2, \quad (2)$$

where  $N$  is the number of atoms of the structure and  $\vec{x}$ ,  $\vec{x}'$  are respectively the positions of the structure under study and its closest achiral reference. Although in later works, Avnir added a normalization factor by the root mean square size of the original centered structure [16] this will not be considered here for simplicity.

One inherent difficulty of the CCM [5, 6] is that it requires selecting the closest non-chiral structure. One may think that a reliable choice would be the non-distorted high symmetry phase, arguing that for small enough distortions, the closest non-chiral configuration is the original reference structure. This simple toy model demonstrates that such an assumption is generally incorrect. In the general case, we can follow a symmetry adapted modes (SAMs) argument. Given a nonchiral high-symmetry phase (R) and a chiral low-symmetry phase (G), one can generally write the total distortion  $\delta$  as the sum over SAMs, namely as  $a\delta_1 + b\delta_2$  where  $\delta_1$  and  $\delta_2$  are the modes associated with the irreducible representations brought up by the  $R \rightarrow G$  transition and  $a$  and  $b$  are real projection coefficients. We can take  $\delta_2$  to be the symmetry breaking mode, while  $\delta_1$  is the mode associated with an isotropy representation of the parent achiral group. Thus the CCM is given by the norm of  $\delta_1$  rather than by the norm of  $\delta$  that would be grater. In fact, the closest non-chiral structure in this example corresponds to the configuration with the octahedral rotation but without the B atom's off-center motion. This problem manifests when computing the CCM with the cubic centrosymmetric structure as a reference. Applying Eq. (2) to our perovskite toy model system with such a reference results in the following value:

$$\text{CCM} = \frac{1}{15} \sum_{i \in \text{atoms}} \|\vec{x}_i - \vec{x}_i^{Pm\bar{3}m}\|^2 = \frac{1}{15} (\xi^2 + 4 \sin^2 \frac{\theta}{2}). \quad (3)$$

We can see that the CCM decouples the off-center motion of the B atom and the octahedra rotation. Therefore, we would obtain a non-zero value if  $\theta$  is non-zero and  $\xi$  is zero or vice-versa, even if we know that we need both distortions simultaneously to have a chiral structure. This is a consequence of the wrong selection of the reference structure. However, if we take as a reference the configuration containing the octahedral rotations, which is the closest non-chiral structure, the CCM would then have a value of

$$\text{CCM} = \frac{1}{15} \sum_{i \in \text{atoms}} \|\vec{x}_i - \vec{x}_i^{I4/mcm}\|^2 = \frac{1}{15} \xi^2, \quad (4)$$

which is not satisfactory either, as much important information is encoded in the selection of the reference

structure, and the value of the final order parameter only relies on the off-centering value of the B atom. Consequently, the chirality contribution measure of two different distortions,  $D_1$  and  $D_2$ , will be higher for the distortion with greater off-centering, regardless of the extent of their octahedral rotations. This discrepancy arises because the reference structures for both distortions differ, potentially leading to misconceptions.

These challenges become more pronounced as the crystal structure becomes more complicated. Identifying the closest non-chiral reference structure can be difficult. While recent numerical approximations, available at [17], have improved computational efficiency to  $N^2$  (compared with the  $N!$  scaling of analytical methods [18]) with an error margin of 2% for cyclic symmetry groups [16], they may disrupt the connectivity map of the structure, resulting in unphysical references [19]. Furthermore, chiral distortions often involve multiple coupled modes in complex systems with many atoms in the unit cell. These modes can become decoupled, as seen in the case where octahedral rotation and the off-centering motion of the B cation are examined separately.

Besides these problem-specific issues, other general problems and considerations about the difficulties of whether continuous chiral measures can be well-defined have been addressed in Ref. [8, 9, 20–22].

## 2. Hausdorff Distances

The Hausdorff distance is defined as the supremum of the minimum distances between the structure and its closest non-chiral reference [1, 10]. Therefore, it also relies on the pre-assumption of a reference structure concerning which computes the supremum of the infimum of the distances (i.e. the supremum for the case of maximal overlap between the structure and the reference). Consequently, the same types of problems discussed above for the CCM are at play too for the Hausdorff distance. When we compute the Hausdorff distance concerning the centrosymmetric structure, we obtain the following value

$$\mathbb{H}(\text{chir}, Pm\bar{3}m) = \sup\{|\xi|, \sin \frac{|\theta|}{2}\}, \quad (5)$$

depending on the values of the off-centering motion and the octahedral rotation, the Hausdorff distance would vary. However, similar to the case of the CCM, since we are computing positive definite distances, no distinction can be made between enantiomers if we reverse either the direction of the rotation or the direction of the off-centering motion. This problematic is common to all scalar measures as mirror symmetries will leave the value unaffected.

Another problem arises With the Hausdorff distance when considering the distances' supremum. For small distortions, the distance between the B atoms is  $\xi$ , and the distance between the equatorial oxygens is  $\sin \frac{\theta}{2} \sim \frac{\theta}{2}$ . Let us imagine that the value of the off-centering and the

rotation is the same. In such a case, the Hausdorff distance would be  $\xi$ . However, the multiplicity of the oxygen atoms is not taken into account. Therefore, even if the overall contribution of the oxygen sites is larger than the one coming from the B atom, as the individual inputs are smaller, they are not considered in the chiral measure. This is an added problem to the ones highlighted above for the case of the CCM.

### 3. Angular Momentum

The angular momentum of a distortion is defined by the sum of the angular momentum of the atomic displacements [23]:

$$\begin{aligned} J &= \frac{1}{N} \sum_{i \in \text{atoms}} m_i \cdot \vec{x}_i \times \dot{\vec{x}}_i, \\ J_z &= \frac{1}{N} \sum_{i \in \text{atoms}} m_i \cdot (x_i^x \dot{x}_i^y - x_i^y \dot{x}_i^x), \\ J_x &= \frac{1}{N} \sum_{i \in \text{atoms}} m_i \cdot (x_i^y \dot{x}_i^z - x_i^z \dot{x}_i^y), \\ J_y &= \frac{1}{N} \sum_{i \in \text{atoms}} m_i \cdot (x_i^z \dot{x}_i^x - x_i^x \dot{x}_i^z), \end{aligned} \quad (6)$$

where  $m_i$  stands for the atomic mass of the  $i$ -th atom,  $\vec{x}_i$  represents its position in the distorted configuration and  $\dot{\vec{x}}_i$  its velocity defined as the difference in position between the distorted and the high-symmetry phases (the difference in positions can be related with a velocity in an arbitrary units of time system following a finite difference approach). In our perovskite toy model system, the velocities of the atoms gives the following values:

$$\begin{aligned} \dot{\vec{x}}_{O_{x1}} &= \left( \frac{1}{2} - \frac{1}{2} \cos \theta, -\frac{1}{2} \sin \theta, 0 \right), \\ \dot{\vec{x}}_{O_{x2}} &= \left( -\frac{1}{2} + \frac{1}{2} \cos \theta, \frac{1}{2} \sin \theta, 0 \right), \\ \dot{\vec{x}}_{O_{y1}} &= \left( \frac{1}{2} \sin \theta, \frac{1}{2} - \frac{1}{2} \cos \theta, 0 \right), \\ \dot{\vec{x}}_{O_{y2}} &= \left( -\frac{1}{2} \sin \theta, -\frac{1}{2} + \frac{1}{2} \cos \theta, 0 \right), \\ \dot{\vec{x}}_B &= (0, 0, \xi). \end{aligned} \quad (7)$$

If we compute the angular momentum for the distortion of Eq. (1) the obtained values are  $J_z = \frac{1}{15} m_O \sin \theta$  irrespective of the off-centering of the B atom, and  $J_x = \frac{1}{15} m_B \frac{\xi}{2}$ ,  $J_y = -\frac{1}{15} m_B \frac{\xi}{2}$  irrespective of the octahedra rotation.

As a pseudovector quantity, angular momentum defies classification as either a scalar or a pseudoscalar measure. Moreover, it lacks the necessary characteristics to serve as a reliable chiral measure, as evidenced by its attribution of non-zero values to achiral structures. Additionally, due to their nature, the rotations of the octahedra and the off-centering of the B atom contribute independently, illustrating a complete decoupling.

## B. Computation of Handedness

Handedness is intrinsically linked to rotational direction in physics. For instance, in chemistry, helicity refers to the sense of rotation of helical structures, with right-handed helices assigned a positive helicity value and left-handed helices assigned a negative helicity value [24]. Similarly, in hydrodynamics, the handedness of a flow is determined by the sign of its helicity, which measures the degree of linkage of the streamlines [13]. This quantity can be computed from the velocity lines of the flow as the following integral [12, 13]:

$$\mathcal{H} = \int d^3r \vec{v} \cdot \left[ \vec{\nabla} \times \vec{v} \right]. \quad (8)$$

The integrand of Eq. (8), the helicity density, is a pseudoscalar quantity that changes its sign under a mirror symmetry operation. Thus, a nonzero helicity is associated with a lack of mirror symmetry: right (respectively left) handedness can be associated with positive (respectively negative) values of  $\mathcal{H}$ . Accordingly, the helicity modulus,  $|\mathcal{H}|$ , quantifies the strength of the handedness [13]. Contrary to scalar measures (like CCM or Hausdorff distances), the helicity measure can discriminate between enantiomers. However, other problems arise due to the chiral connectedness property [25–28]. This property refers to the fact that two enantiomorphs can be transformed into one another while remaining chiral throughout the transformation process. As elucidated in Ref. [25–27], this inevitably leads to what is known as the *false zeros problem*: Any pseudoscalar function will, in general, fail to determine the handedness of some objects assigning zero values to chiral entities. A notable exception to the false-zeros problem occurs in the set of helices with variable pitch, as discussed in Ref. [29]. In these cases, pseudoscalar functions exclusively yield zero values for achiral objects, making them suitable measures of chirality. Consequently, enantiomorphic space groups are unaffected by this issue and can be classified according to their handedness, indicating that pseudoscalar functions are more convenient for such classifications. Conversely, non-enantiomorphic space groups showing chirality like the  $\text{Pb}_5\text{Ge}_3\text{O}_{11}$  compound [30], may exhibit chiral connectedness, making the presence of chiral non-handed configurations inevitable.

Inspired by this definition, we shall try to apply it to our particular problem where a continuous distortion can be established between the achiral and chiral phases. In such a case, the velocity field can be defined, as in the case of the angular momentum, by the individual atomic displacements from the high-symmetry phase to the low-symmetry chiral phase (i.e., going from continuous to discrete vector fields). The curl  $\vec{\nabla} \times \dot{\vec{x}}_i$ , is then computed following a finite difference approach and the integral is substituted by a regular sum at each atomic site. Note that whenever this field cannot be established as it is the case for instance of reconstructive phase transition this method cannot be applied. With this definition and the



set of velocities described in Eq. (7), we obtain a value of the helicity of:

$$\mathcal{H} = \sin \theta \cdot \xi. \quad (9)$$

Therefore, to have a non-zero helicity, we need the coupling of the oxygen rotation and the polar displacement, as desired, to characterize a chiral structure. Moreover, suppose we reverse the sense of rotation or the sign of the polar distortion inducing a change of handedness in the structure. In that case, the helicity changes sign accordingly in contrast to the scenario observed with the CCM or Hausdorff distances.

In the following sections, we shall apply this method (available at [31]) to compute the handedness of different crystalline structures that undergo such continuous chiral transitions. Although not used in these computations, a reciprocal space formulation is indeed possible, allowing its incorporation within DFPT methods and finite wavelength approaches. As proven in Appendix A, the helicity equals the value at  $\Gamma$  of the Fourier transform of the helicity density operator,

$$\hat{H}(\vec{k}) = \mathcal{F}[\vec{v}] \star (i\vec{k} \times \mathcal{F}[\vec{v}]), \quad (10)$$

where  $\mathcal{F}$  stands for the Fourier transform and  $\star$  is defined as the component wise convolution operator.

### III. APPLICATION TO $\text{K}_3\text{NiO}_2$ LIKE CHIRAL STRUCTURE

One interesting application case is found in the  $\text{K}_3\text{NiO}_2$  compound [32]. At 423 K, this crystal exhibits a first-order chiral phase transition from a high-symmetry achiral phase ( $P4_2/mnm$  space group) to a low-symmetry enantiomorphic phase (either  $P4_12_12$  or  $P4_32_12$ ). The transition is continuous and has been identified to come from a zone boundary soft phonon mode that explains the cell doubling during the transition [33]. Such a phenomenon could be present in all crystals that can be stabilized into the same high-symmetry  $P4_2/mnm$  crystal structure. For example, although  $\text{Na}_3\text{AuO}_2$  does not crystallize in this structure, a hypothetical  $\text{Na}_3\text{AuO}_2$  phase isostructural to  $\text{K}_3\text{NiO}_2$  is a useful non-magnetic and closed shell toy model system for computational studies. In this section, we shall compute the CCM, Hausdorff distances, angular momentum, and chirality for  $\text{K}_3\text{NiO}_2$  and  $\text{Na}_3\text{AuO}_2$ . The latter is much simpler from a computational perspective due to its non-magnetic nature. It will be used to systematically analyze how the different chirality measures behave when connecting the different possible phases. In Fig. 2, we show a schematic representation of the  $\text{K}_3\text{NiO}_2$  crystal. Atomic positions correspond to the high-symmetry  $P4_2/mnm$  phase, and the arrows indicate how the atoms move when transitioning to the chiral  $P4_12_12$  phase. In that way, we have defined a vector field for every atomic site in the reference structure, and therefore, we can compute all the quantities discussed in previous sections. We

can see from the arrows plotted in Fig. 2 that a handed helical distortion pattern along the  $c$ -direction is present.

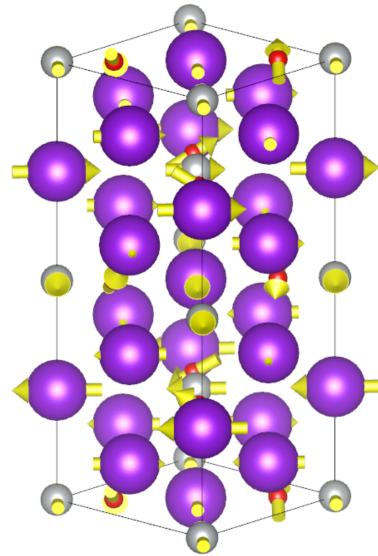


FIG. 2. Schematic representation of the  $\text{K}_3\text{NiO}_2$  crystal structure where atoms occupy the  $P4_2/mnm$  high symmetry positions. Arrows indicate the direction of the atom displacements that bring the system to the  $P4_32_12$  chiral phase. Purple, grey, and red balls represent K, Ni, and O atoms

TABLE I. Values of the different chirality measures discussed before for the  $\text{Na}_3\text{AuO}_2$  compound taking the  $P4_2/mnm$  phase as a reference. The + and - superscripts represent the enantiomorphic  $P4_12_12$  and  $P4_32_12$  phases, respectively. Fractional units and normalization by the number of atoms in the unit cell have been used to compute the CCM, angular momentum, and helicity. The  $z$  component of the angular momentum is zero in both enantiomers and is omitted for brevity.

	$\text{Na}_3\text{AuO}_2^+$	$\text{Na}_3\text{AuO}_2^-$
CCM	3.30e-3	3.30e-3
Hausdorff	1.18e-1	1.18e-1
Angular Momentum	[1.27e-3; 5.73e-3]	[5.89e-3; 1.43e-3]
Helicity	7.75e-3	-7.75e-3

As we can see in Tab. I for the case of  $\text{Na}_3\text{AuO}_2$ , the values of the CCM and Hausdorff distances calculations give each the same value for both enantiomers, which is in line with what we discussed before in Sec. II A, i.e. that these measures cannot distinguish two enantiomers as distances are always positive definite. When we reverse the structure's chirality, the angular momentum calculation shows a rotation change between the two enantiomeric phases. This is because both enantiomers are related by a mirror symmetry along  $\hat{n} = [110]$  and

therefore the mirror symmetry matrix takes the form

$$M = \mathbb{I} - 2\hat{n}^t\hat{n} = \begin{pmatrix} 0 & -1 & 0 \\ -1 & 0 & 0 \\ 0 & 0 & 1 \end{pmatrix}, \quad (11)$$

which applied to the angular momentum formulae results in a  $x \leftrightarrow y$  permutation.

Finally, the sign of helicity is sensitive to the system's change of handedness while its modulus is constant. Hence, and as anticipated in Sec. II B, the helicity modulus can measure the chiral distortion amplitude while its sign encodes the handedness "sign" of the structure.

To compare those different measures, we plot in Fig. 3 the evolution of the CCM, Hausdorff, and helicity measures as a function of the distortion amplitude when going from the high symmetry  $P4_2/mnm$  phase to both the  $P4_12_12$  and  $P4_32_12$  phases. Those two phases are degenerate in energy and correspond to the two energy minima of the left and right-handed enantiomers that can be formed from the  $P4_2/mnm$  phase. The difference in the distortion pattern of those two enantiomeric phases is simply a change of sign, i.e., a change between right-handed and left-handed helical distortion. As expected from the different definitions, the module of the Hausdorff distance shows a linear dependence with  $\eta$ . In contrast, the module of the CCM and the helicity measurements have a quadratic behavior, as already reported in Ref. [1]. Moreover, as anticipated, the helicity sign is reversed for the different enantiomers, whereas the CCM and Hausdorff distances are not.

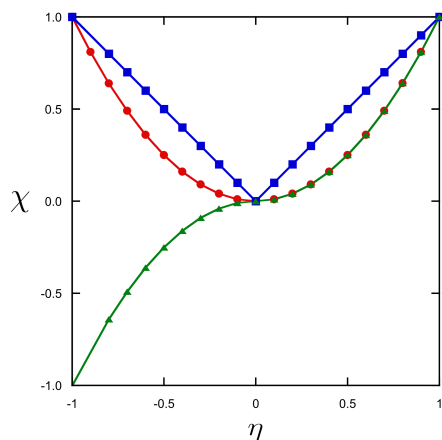


FIG. 3. Comparison of the evolution of the different chiral measures as a function of the amplitude of the chiral distortion  $\eta$  in  $\text{Na}_3\text{AuO}_2$ . Positive (negative) values of  $\eta$  correspond to the condensation of the modes towards the  $P4_12_12$  ( $P4_32_12$ ) phase. Red dots, blue squares, and green triangles correspond to CCM, Hausdorff, and Helicity measures.

Furthermore, when assessing the same calculations between the  $P4_2/mnm$  phase and the  $Cmcm$  intermediate achiral phase, which is found to be an intermediate

achiral structure before the enantiomorphous groups [33], we obtain a zero value from the helicity calculation. Therefore, the helicity calculation appears robust in determining the chirality of helical structures and can be applied straightforwardly. Moreover, as one can see in Tab. II, when we apply this procedure to the case of the  $\text{K}_3\text{NiO}_2$  and compare the results with the ones obtained for the  $\text{Na}_3\text{AuO}_2$ , we observe that the ratio between of the CCM's and the ratio of the helicities is constant suggesting the same helical structure for both compounds.

#### IV. THE CASE OF $\text{CsCuCl}_3$

Next, we will discuss the chiral transition in  $\text{CsCuCl}_3$ . This material undergoes a transition from a high-temperature, high-symmetry  $P6_3/mmc$  phase to one of the enantiomorphous groups  $P6_122$  or  $P6_522$ [34, 35]. This transition is driven by a cooperative Jahn-Teller distortion as reported in Ref. [36, 37]. Figure 4 illustrates a schematic representation of the  $\text{CsCuCl}_3$  crystal, similar to our previous example. It shows the chiral crystal distortions, depicted as differences in atomic positions between the high-symmetry phase and one of the chiral phases. The displacement vector field demonstrates the right-handed helical structure. In Tab. II, the values of the different chirality measures can be encountered compared to other compounds. As we can see from the data, if we compare the values of the different measures for the  $\text{Na}_3\text{AuO}_2$  and the  $\text{CsCuCl}_3$  cases, we can see that the ratio between the CCM is half of the ratio between the helicities, indicating that the  $\text{CsCuCl}_3$  adopts a more pronounced helical structure at equal distortion.

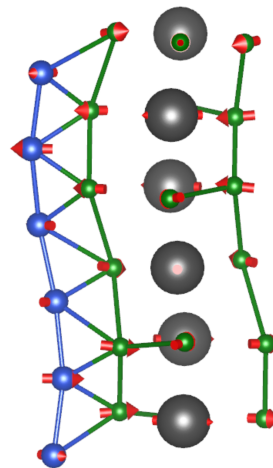


FIG. 4. Schematic representation of the  $\text{CsCuCl}_3$  where atoms occupy the high symmetry positions. Arrows indicate the direction of the displacements into the  $P6_122$  chiral phase. Grey, blue, and green balls represent Cs, Cu, and Cl atoms.

TABLE II. Values of the different chirality measures for the distinct compounds discussed in the work. Fractional units and normalization by the number of atoms in the unit cell have been performed to compute the CCM, angular momentum, and helicity.

	Na <sub>3</sub> AuO <sub>2</sub>	K <sub>3</sub> NiO <sub>2</sub>	CsCuCl <sub>3</sub>	MgTi <sub>2</sub> O <sub>4</sub>
CCM	3.30e-3	1.24e-3	5.66e-3	1.03e-4
Hausdorff	1.18e-1	7.35e-2	1.07e-1	1.19e-2
Angular Momentum	[1.27e-3; 5.73e-3; 0.00]	[2.25e-3; 6.75e-3; 0.00]	[1.07e-2; -6.50e-3; 0.00]	[-1.29e-3; 3.27e-4; 0.00]
Helicity	7.75e-3	2.75e-3	2.08e-2	3.08e-4

## V. THE CASE OF MgTi<sub>2</sub>O<sub>4</sub>

A crucial prerequisite for computing the helicity of a given structure is the ability to establish a one-to-one mapping between atomic positions in the high symmetry phase and those in the low symmetry phase, thereby defining the displacement vector field. In previous examples, establishing this mapping has been straightforward. However, in the case of MgTi<sub>2</sub>O<sub>4</sub>, this is not so. The high-temperature phase exhibits a structure of  $Fd-3m$  symmetry with 56 atoms in the conventional unit cell. In contrast, the chiral phase exhibits a  $P4_12_12$  or  $P4_32_12$  space group symmetry with 28 atoms in the unit cell [38, 39]. To establish such a mapping, we used the ISODISTORT software[40, 41]. Beginning with the high symmetry phase and setting the distortions that bring the system to the  $P4_12_12$  or  $P4_32_12$  phase to zero, we could derive a set of undistorted atomic positions that adhere to the desired symmetry. Afterward, we provided to AMPLIMODES[42, 43] the undistorted and distorted atomic coordinates to obtain the set of displacements. In Fig. 5, we present the atomic displacements obtained using this method.

Similar to previous examples, the CCM and Hausdorff distances are equivalent for both enantiomers, while the helicity exhibits the same magnitude but opposite signs between them. The numerical values of the different chirality quantification methods can be found in Tab. II. In comparison to the Na<sub>3</sub>AuO<sub>2</sub> case, the ratio between the CCM values roughly equals the ratio between the helicities, suggesting that the two compounds present approximately the same chiral strength. In contrast to the previously discussed cases where a clear helical structure was observable along the  $c$ -direction, this compound exhibits a more evenly distributed helicity due to the lattice's transition from a face-centered cubic to a tetragonal structure. The corresponding distortion results in the absence of a preferred direction, making it more difficult to identify the helical structure of the compound visually.

## VI. CONCLUSIONS

In this work, we have delved into various continuous chirality measures proposed in the literature. Utilizing the simple model system of a unit perovskite cell, we

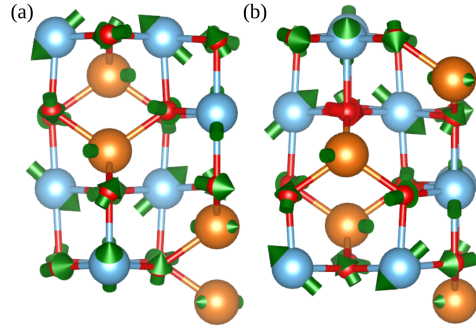


FIG. 5. Schematic representation of the MgTi<sub>2</sub>O<sub>4</sub>. Atoms occupy the high symmetry undistorted positions in a (a)  $P4_12_12$  or (b)  $P4_32_12$  representation. Arrows indicate the direction of the displacements into their respective chiral phases. Orange, blue and red balls represent Mg, Ti and O atoms respectively.

have examined the challenges these measures pose when applied to extended solids. For the case of the CCM or Hausdorff distances, in addition to the difficulties associated with employing a position-based operator in periodic systems [44], not discussed in the text, we have identified the critical issue of selecting an appropriate reference, which can often be non-trivial. Even in the case of small chiral distortions, relying on the high-symmetry phase as an accurate reference may not suffice, as the deformation could involve multiple non-chiral modes that only become chiral when coupled together as exemplified by the rotation (axial-like) and off-centering (vector) distortions. Consequently, much important information about the distortion can remain implicitly hidden even with the right reference selection. Moreover, because these methods rely on computing distances, which are positive definite quantities, they cannot discriminate between the different enantiomorphic structures of a given compound.

Regarding the angular momentum, we show how it can provide non-zero values for non-chiral distortions, being, therefore, difficult to attest to the effectiveness of such an approach. Despite this limitation, unlike the CCM or Hausdorff distances, the angular momentum will yield distinct values for each enantiomorph. As demonstrated in Section III, the relationship between the values of the two enantiomorphs will be determined by the mirror symmetry that connects them.

Besides the analysis of the various chirality measures

in the literature [8], we have proposed using a novel pseudoscalar function, the helicity, to quantify the handedness of solids that undergo a continuous transition from an achiral to a chiral enantiomorphic space group. Borrowing the definition from hydrodynamics [12, 13], this quantity can be directly computed from the eigenvector that brings the system from the high-symmetry non-chiral phase to the low-symmetry chiral one. We have demonstrated the method’s robustness in measuring the handedness of a given distortion in enantiomorphic groups that do not suffer the false zeros problem. In such groups, helicity not only yields zero values for non-chiral transformations but also provides finite values for chiral structures, with equal magnitude and opposite signs for each enantiomorph. Such approach has unveiled the handedness of different compounds like  $\text{Na}_3\text{AuO}_2$ ,  $\text{CsCuCl}_3$  or  $\text{MgTi}_2\text{O}_4$ . The use of helicity as defined in the article would be therefore potentially interesting to characterize chiral phonons [45]. While effective in measuring the handedness of crystals with enantiomorphic space groups (the 11 enantiomorphic pairs), it is important to note that chiral crystals that are within the 43 non-enantiomorphic space groups present chiral-connectedness such that this approach may be inadequate in those cases enhancing the well-known difference between chirality and handedness [1]. Finally, we anticipated a reciprocal space formulation allowing its incorporation within density functional perturbation methods and finite wavelength approaches [46].

Even though the helicity described in this article remains reliant on a position-based operator and thus susceptible to common challenges in dealing with periodic systems [44], we hope that our proposed approach will facilitate a more systematic quantification of crystal handedness of enantiomorphic space groups and stimulate further work towards refining the quantification of structural chirality. For instance, it would be interesting to establish a relation between helical structures’ helicity from enantiomorphic groups and their optical activity, e.g., from density functional theory as the optical activity calculation has been recently implemented [47].

## ACKNOWLEDGMENTS

F.G.-O., M.F. and E.B. acknowledge the Fonds de la Recherche Scientifique (FNRS) for financial support, the PDR project CHRYSALID No.40003544 and the Consor-

tium des Équipements de Calcul Intensif (CÉCI), funded by the F.R.S.-FNRS under Grant No. 2.5020.11 and the Tier-1 Lucia supercomputer of the Walloon Region, infrastructure funded by the Walloon Region under the grant agreement No. 1910247. F.G.-O. and E. B. also acknowledge support by the European Union’s Horizon 2020 research and innovation program under Grant Agreement No. 964931 (TSAR). The work at West Virginia University was supported by the U.S. Department of Energy (DOE), Office of Science, Basic Energy Sciences (BES), under Award DE-SC0021375. This work used Bridges2 and Expanse at the Pittsburgh Supercomputer and the San Diego Supercomputer Center through allocation DMR140031 from the Advanced Cyberinfrastructure Coordination Ecosystem: Services & Support (ACCESS) program, which National Science Foundation supports grants 2138259, 2138286, 2138307, 2137603, and 2138296.

## Appendix A: Reciprocal space formulation of the Helicity

This short section is devoted to the straightforward demonstration of Eq. (10). First, it is clear that the value at  $\Gamma$  of the Fourier transform of the helicity density operator corresponds to the helicity.

$$\begin{aligned}\hat{H}(\vec{k} = 0) &= \int \vec{v} \cdot (\nabla \times \vec{v}) \cdot e^{i\vec{0}\cdot\vec{r}} d^3\vec{r} \\ &= \int \vec{v} \cdot (\nabla \times \vec{v}) \cdot 1 d^3\vec{r} = \mathcal{H}.\end{aligned}$$

Now, we only have to compute the Fourier transform of the helicity density operator  $\hat{H}(\vec{r}) = \vec{v} \cdot (\nabla \times \vec{v})$ . Applying the convolution theorem [48], the Fourier transform of the product of two vectorial functions corresponds to the component-wise convolution of their respective Fourier transforms. Therefore, the following equality holds

$$\mathcal{F}[\vec{v} \cdot (\nabla \times \vec{v})] = \mathcal{F}[\vec{v}] \star \mathcal{F}[\nabla \times \vec{v}]. \quad (\text{A1})$$

Moreover, the Fourier transform of the curl of a function can be rewritten in the following way [48]

$$\mathcal{F}[\nabla \times \vec{v}] = i\vec{k} \times \mathcal{F}[\vec{v}], \quad (\text{A2})$$

which completes the prove of Eq. (10).

---

[1] G. H. Fecher, J. Kübler, and C. Felser, Chirality in the solid state: Chiral crystal structures in chiral and achiral space groups, *Materials* **15**, 10.3390/ma15175812 (2022).  
 [2] M. Nespolo, M. I. Aroyo, and B. Souvignier, Crystallographic shelves: space-group hierarchy explained, *Journal of Applied Crystallography* **51**, 1481 (2018).

[3] E. Bousquet, M. Fava, Z. Romestan, F. Gómez-Ortiz, E. E. McCabe, and A. H. Romero, Structural chirality and related properties in the periodic inorganic solids: Review and perspectives, To be published (2024).  
 [4] M. Parker, *Physics of Optoelectronics*, ISSN (CRC Press, 2018).



- [5] H. Zabrodsky, S. Peleg, and D. Avnir, Continuous symmetry measures, *J. Am. Chem. Soc.* **114**, 7843 (1992).
- [6] H. Zabrodsky and D. Avnir, Continuous symmetry measures. 4. Chirality, *J. Am. Chem. Soc.* **117**, 462 (1995).
- [7] N. Weinberg and K. Mislow, On chirality measures and chirality properties, *Can. J. Chem.* **78**, 41 (2000).
- [8] M. Petjean, Chirality and symmetry measures: A transdisciplinary review, *Entropy* **5**, 271 (2003).
- [9] P. W. Fowler, Quantification of chirality: Attempting the impossible, *Symmetry: Cult. Sci.* **16**, 321 (2005).
- [10] A. B. Buda and K. Mislow, A Hausdorff chirality measure, *J. Am. Chem. Soc.* **114**, 6006 (1992).
- [11] S. Streib, Difference between angular momentum and pseudoangular momentum, *Phys. Rev. B* **103**, L100409 (2021).
- [12] H. Moffatt and R. Ricca, Helicity and the Călugăreanu invariant, *Proc. R. Soc. Lond. A* **439**, 411 (1992).
- [13] H. K. Moffatt, Helicity and singular structures in fluid dynamics, *Proc. Natl. Acad. Sci. U.S.A.* **111**, 3663 (2014).
- [14] M. Nespolo and A. H. Benahsene, Symmetry and chirality in crystals, *J. Appl. Crystallogr.* **54**, 1594 (2021).
- [15] J. Hlinka, Eight types of symmetrically distinct vectorlike physical quantities, *Phys. Rev. Lett.* **113**, 165502 (2014).
- [16] C. Dryzun, A. Zait, and D. Avnir, Quantitative symmetry and chirality—a fast computational algorithm for large structures: Proteins, macromolecules, nanotubes, and unit cells, *Journal of Computational Chemistry* **32**, 2526 (2011).
- [17] A. Zayit, M. Pinsky, H. Elgavi, C. Dryzun, and D. Avnir, A web site for calculating the degree of chirality, *Chirality* **23**, 17 (2011).
- [18] M. Pinsky, C. Dryzun, D. Casanova, P. Alemany, and D. Avnir, Analytical methods for calculating continuous symmetry measures and the chirality measure, *Journal of Computational Chemistry* **29**, 2712 (2008).
- [19] G. Alon, Y. Ben-Haim, and I. Tuvi-Arad, Continuous symmetry and chirality measures: approximate algorithms for large molecular structures, *Journal of Cheminformatics* **15**, 106 (2023).
- [20] A. B. Buda, T. A. der Heyde, and K. Mislow, On quantifying chirality, *Angew. Chem. Int. Ed. Eng.* **31**, 989 (1992).
- [21] G. Gillat, On quantifying chirality – obstacles and problems towards unification, *J. Math. Chem.* **15**, 197 (1994).
- [22] S. J. Jenkins, *Chirality at Solid Surfaces* (John Wiley & Sons, Ltd, 2018).
- [23] L. Zhang and Q. Niu, Angular momentum of phonons and the einstein-de haas effect, *Phys. Rev. Lett.* **112**, 085503 (2014).
- [24] G. P. Moss, Basic terminology of stereochemistry (iupac recommendations 1996), *Pure Appl. Chem.* **68**, 2193 (1996).
- [25] P. G. Mezey, Rules on chiral and achiral molecular transformations, *J. Math. Chem.* **17**, 185 (1995).
- [26] N. Weinberg and K. Mislow, On chiral pathways in: A dimensional analysis, *Theor. Chim. Acta* **95**, 63 (1997).
- [27] M. Banik, K. Rodriguez, E. Hulkko, and V. A. Apkarian, Orientation-dependent handedness of chiral plasmons on nanosphere dimers: How to turn a right hand into a left hand, *ACS Photonics* **3**, 2482 (2016).
- [28] M. Vavilin and I. Fernandez-Corbaton, Multidimensional measures of electromagnetic chirality and their conformal invariance, *New J. Phys.* **24**, 033022 (2022).
- [29] K. Mislow, Molecular chirality, in *Topics in Stereochemistry* (John Wiley & Sons, Ltd, 1999) pp. 1–82.
- [30] M. Fava, W. Lafargue-Dit-Hauret, A. H. Romero, and E. Bousquet, Ferroelectricity and chirality in the  $\text{pb}_5\text{ge}_3\text{o}_{11}$  crystal, *Phys. Rev. B* **109**, 024113 (2024).
- [31] F. Gómez-Ortiz, Helicity computation, [https://github.com/Gomez-OrtizF/Helicity\\_Computation\\_Crystals/](https://github.com/Gomez-OrtizF/Helicity_Computation_Crystals/) (2024).
- [32] K. Duriš, U. Müller, and M. Jansen,  $\text{K}_3\text{NiO}_2$  revisited, phase transition and crystal structure refinement, *Z. Anorg. Allg. Chem.* **638**, 737 (2012).
- [33] M. Fava, E. McCabe, A. H. Romero, and E. Bousquet, A phonon-driven mechanism for an emergent and reversible chirality in crystals (2024), [arXiv:2405.12696](https://arxiv.org/abs/2405.12696) [cond-mat.mtrl-sci].
- [34] T. Koiso, K. Yamamoto, Y. Hata, Y. Takahashi, E. Kita, K. Ohshima, and F. P. Okamura, Determination of the chiral structure of using anomalous x-ray scattering near the cs k absorption edge, *J. Phys. Condens. Matter* **8**, 7059 (1996).
- [35] V. P. Plakhty, J. Wosnitza, N. Martin, Y. Marchi, O. P. Smirnov, B. Grenier, and S. V. Gavrilov, Isostructural transition coupled with spin ordering in  $\text{CsCuCl}_3$ : A spatially frustrated spiral crystal lattice, *Phys. Rev. B* **79**, 012410 (2009).
- [36] C. Kroese and W. Maaskant, The relation between the high-temperature and room-temperature structure of  $\text{CsCuCl}_3$ , *Chemical Physics* **5**, 224 (1974).
- [37] S. Hirotsu, Jahn-Teller induced phase transition in  $\text{CsCuCl}_3$ : structural phase transition with helical atomic displacements, *J. Phys. C: Solid State Phys.* **10**, 967 (1977).
- [38] M. Schmidt, W. Ratcliff, P. G. Radaelli, K. Refson, N. M. Harrison, and S. W. Cheong, Spin singlet formation in  $\text{MgTi}_2\text{O}_4$ : Evidence of a helical dimerization pattern, *Phys. Rev. Lett.* **92**, 056402 (2004).
- [39] V. V. Ivanov, V. M. Talanov, V. B. Shirokov, and M. V. Talanov, Crystal chemistry and formation mechanism of tetragonal  $\text{MgTi}_2\text{O}_4$ , *Inorganic Materials* **47**, 990 (2011).
- [40] H. T. Stokes, D. M. Hatch, and B. J. Campbell, ISODIS-TORT, ISOTROPY software suite, [iso.byu.edu](http://iso.byu.edu).
- [41] B. J. Campbell, H. T. Stokes, D. E. Tanner, and D. M. Hatch, *ISODISPLACE*: a web-based tool for exploring structural distortions, *J. Appl. Crystallogr.* **39**, 607 (2006).
- [42] D. Orobengoa, C. Capillas, M. I. Aroyo, and J.-M. Perez-Mato, *AMPLIMODES*: symmetry-mode analysis on the Bilbao Crystallographic Server, *J. Appl. Crystallogr.* **42**, 820 (2009).
- [43] J. M. Perez-Mato, D. Orobengoa, and M. I. Aroyo, Mode crystallography of distorted structures, *Acta Crystallogr. A* **66**, 558 (2010).
- [44] R. Resta, Quantum-mechanical position operator in extended systems, *Phys. Rev. Lett.* **80**, 1800 (1998).
- [45] H. Ueda, M. García-Fernández, S. Agrestini, C. P. Romao, J. van den Brink, N. A. Spaldin, K.-J. Zhou, and U. Staub, Chiral phonons in quartz probed by x-rays, *Nature* **618**, 946 (2023).
- [46] M. Royo and M. Stengel, First-principles theory of spatial dispersion: Dynamical quadrupoles and flexoelectricity, *Phys. Rev. X* **9**, 021050 (2019).
- [47] A. Zabalo and M. Stengel, Natural optical activity from density-functional perturbation theory, *Phys. Rev. Lett.* **131**, 086902 (2023).

- [48] G. van Dijk, *Distribution Theory: Convolution, Fourier Transform, and Laplace Transform* (De Gruyter, Berlin, Boston, 2013).